Au on Ag/Si(111)-($\sqrt{3}\times\sqrt{3}$)$R30°$: A spectromicroscopy study of a bimetal-silicon interface

S. Günther, A. Kolmakov, J. Kovac,* M. Marsi, and M. Kiskinova
Sincrotrone Trieste, Padriciano 99, 34012 Trieste, Italy
(Received 20 January 1997)

We present a scanning-photoemission-microscopy study of the Au on Ag/Si(111)-($\sqrt{3}\times\sqrt{3}$)$R30°$ interface containing two different phases: a two-dimensional (2D) ordered surface with additional three-dimensional Ag islands. Our submicrometer lateral resolution makes it possible to characterize these two phases in function of Au coverage and annealing temperature. On the 2D ($\sqrt{3}\times\sqrt{3}$)$R30°$-Ag/Si regions no major disruption of the ordered structure occurs for Au coverages up to $\frac{2}{3}$ ML, where a ($2\sqrt{3}\times 2\sqrt{3}$)$R30°$ low-energy electron-diffraction (LEED) pattern can be observed after annealing at 470 K. If this Au coverage is exceeded, exchange processes between Ag and Au atoms take place on the 2D phase, resulting in an amorphous Au/Si interface with small Ag clusters on top; annealing this interface restores the ($\sqrt{3}\times\sqrt{3}$)$R30°$ LEED pattern which, on the basis of our core-level and valence-band spectra, we assign to a ($\sqrt{3}\times\sqrt{3}$)$R30°$ reconstruction similar to the initial one. This suggests the transport of Au toward the 3D phase, where Ag-Au alloying is the dominating process. Strong Au-Ag interactions take place on the 3D islands already at low Au coverages and even at room temperature. The Si skin, which is originally present on the 3D islands, is penetrated by Au and is also maintained after annealing. Finally, the different electronic properties of the two phases, in particular the evolution of the initially semiconducting 2D phase, could be shown by detecting their valence-band electronic structure. [S0163-1829(97)07531-0]

I. INTRODUCTION

Ag/Si(111) and Au/Si(111) systems have been among the most intensively studied metal-semiconductor interfaces during the last two decades.[1–10] It was found that, despite their structural similarity, the electronic structures of the ordered two-dimensional (2D) ($\sqrt{3}\times\sqrt{3}$)$R30°$ phases (called the $\sqrt{3}$-phase from now on) of Au and Ag differ substantially: the density of states near the Fermi level in the valence-band spectra classified the $\sqrt{3}$-Au/Si(111) as metallic, and the $\sqrt{3}$-Ag/Si(111) as semiconducting.[9,10] Even though the structure and properties of the $\sqrt{3}$-Ag/Si(111) and $\sqrt{3}$-Au/Si(111) interfaces have been very thoroughly studied, it is only recently that the chemical shift of the Ag $3d$ core levels has been measured.[11] In most cases the formation processes of these metal interfaces result in the formation and coexistence of 2D ordered and metal-rich three-dimensional phases. Since the properties of the interfaces depend on their structural quality, the role of the different subphases in the formation process has to be clarified.

Surprisingly little is known about the variations in the surface and near-surface chemical composition and the electronic structure of the 3D phases. This is because these phases often are of submicron size and cover a small fraction of the surface, which requires surface-sensitive techniques combining high spatial resolution and chemical sensitivity. High spatial resolution and sufficient energy resolution to locally probe the composition of the coexisting subphases are provided by the scanning photoelectron microscope (SPEM) at the ELETTRA synchrotron radiation source.[11] Quite recently, SPEM studies with a submicrometer resolution revealed the complex composition of the 3D phases at Au/Si(111) and Ag/Si(111) interfaces.[12,13] It was found that the 3D metal agglomerates are usually covered by metal silicide and unreacted Si skin on top, the thickness of this cover depending on the metal coverage, the type of the metal, and the formation temperature.

Much scarcer is information on the electrical properties and composition of bimetal (Au+Ag)/Si interfaces, where the structural studies showed a great variety of ordered 2D and agglomerated 3D islands.[14–16] To our best knowledge, both subphases of these bimetal interfaces lack a quantitative characterization of the surface and near-surface composition, as far as concentration, electronic structure, and chemical state of the interface constituents. This limits the understanding of the formation processes in bimetal systems, which is of great importance for device technology. For example, it is not clear how Ag impurities can affect the thermal stability and the electrical properties of the commonly used Au/Si contacts. In our recent paper on the evolution of a morphologically complex Au/Si(111) surface after deposition of Ag, we showed that the presence of metallic Au in the 3D phase determines its higher reactivity to Ag-Au alloying, the main process controlling the evolution of the morphologically complex Au/Si interface after deposition of Ag.[17] Since previous structural studies reported that the Au-Ag deposition sequence resulted in a different evolution of the bimetal interface, we expanded our study on the coverage and temperature effects observed during the interaction of Au with a morphologically heterogeneous Ag/Si(111) interface. Indeed, it turned out that this formation mode results in a greater variety of events. As manifested by our spatially resolved core level and valence spectra, in addition to AgAu alloying other factors play an important role in the different stages of the formation process, such as the higher affinity of Au to Si, the energetics involved in $\sqrt{3}$-Au and $\sqrt{3}$-Ag reconstructions, Ag mobility, and Au agglomeration.

II. EXPERIMENT

The experiments were performed at the ESCA Microscopy beamline on the ELETTRA synchrotron radiation

source.[12] The measurement station consists of several subchambers hosting a scanning photoemission microscope, and facilities for preparation and characterization of the specimen before transporting in the SPEM. The photon beam provided by an undulator and monochromatized by a spherical grating monochromator was demagnified in the SPEM to a spot of 0.15 μm diameter by using a zone plate optical system. The emitted photoelectrons were collected by a 100-mm hemispherical analyzer with a large acceptance angle, mounted at 70° with respect to the sample normal and the incident photon beam. Elemental or chemical mapping was performed by scanning the sample with respect to the focused beam with the analyzer tuned to the desired kinetic energy. In the normal energy distribution mode, photoelectron (PE) core or valence spectra were recorded from spots on features selected from the maps. All measurements in the present study were carried out with a photon energy of 490 eV, which is a good compromise between the sample-optics working distance ($\sim$7 mm), photoelectron yield ($\sim$1000 counts/s), and energy resolution (0.4 eV).

An n-type Si(111) wafer (0.017 Ω cm) mounted on Ta clips was resistively heated up to 1450 K to prepare a Si(111)-(7×7) surface. Resistively heated tungsten baskets containing a Ag (or Au) droplet were used as metal evaporators. The sample temperature was measured with an optical pyrometer calibrated against a thermocouple in a separate experiment. After each metal evaporation or annealing step the structure and composition of the interface was characterized by low-energy electron diffraction (LEED), Auger electron spectroscopy, and SPEM.

The initial $\sqrt{3}$-Ag/Si interface containing 3D Ag adislands was prepared by evaporating 2–4 ML Ag on to the Si(111)-(7×7) surface at 300 K, followed by annealing up to 793 K for 15 min. 1 ML equals the (1×1)-Si(111) surface density, 7.8×10^{14} atoms/cm^2. Besides the SPEM, the reproducibility in the morphology of the produced Ag/Si interfaces and their structural quality was controlled *ex situ* using a scanning electron microscope (SEM, JEOL 5400). The higher spatial resolution of the SEM ($\sim$10 nm) allowed us to detect existence of smaller 3D islands which cannot be observed by the SPEM. The SPEM and SEM images showed that after a sufficient annealing time (15 min) the $\sqrt{3}$-Ag/Si surface contained $\leqslant$micrometer-sized 3D islands of height $\sim$500 Å.[8,18] The 3D islands cover only $\leqslant$1% of the $\sqrt{3}$-Ag surface, which appears in the images as a flat and homogeneous 2D phase.

For fitting the PE core-level spectra of Au, Ag, and Si we used the reference Au 4f and Ag 3d spectra from the clean metal Au or Ag films deposited on the Ta clips and the Si 2p spectra of the (7×7)-Si(111) surface. Lorentzian, Gaussian, and Doniach-Sunjic functions were used for fitting the spectra. The fitting parameters used in the present paper are summarized in Table I.

For quantitative evaluations from the experimental peak intensities I_x, we used first procedures which corrected for the difference in the core-level photoionization cross sections S_x. By dividing I_x by S_x, the signal I_x/S_x becomes proportional to the number of the photoemitting atoms x. In the present multicomponent system we applied normalization dividing I_x/S_x to the sum of the cross-section-corrected core-level peak intensities of all elements at the interface (Au 4f, Ag 3d, and Si 2p in the present case). In this manner the photon flux variations source are automatically accounted for. To calculate the composition and the thickness of the interface, we have to consider the signal contribution from deeper layers, which is determined by the effective mean free path (EMFP) of the emitted electrons. For our experimental setup we estimated the following values for the attenuation length λ: 8 or 12 Å for Si 2p, 8 Å for Au 4f, and 5 Å for Ag 3d photoelectrons. The two values for Si come from the difference between the universal curve values[19] and the tables of Ref. 20, and can be regarded as the main source for uncertainties in the quantification of the results. In order to account for that, we used always as reference points the Ag 3d, Au 4f, and Si 2p intensities measured for the $\sqrt{3}$-Ag/Si and $\sqrt{3}$-Au/Si interfaces, containing 1 ML noble metal atoms.[4,6,21,22] Depending on the used values for the EMFP, we can adjust the sensitivity factors so that the normalized Si 2p intensities are consistent with the attenuation due to 1 ML noble metal on top the Si(111) surface. Thus the accuracy of the quantitative evaluations are rather precise (10%) regarding the 2D phase. Larger errors (up to 50%) can be made in quantification of the surface and near-surface layers of the 3D phase, where the stoichiometry can change with depth.

TABLE I. Fitting parameters for the Ag 3d and Au 4f core-level peaks.

	Spin-orbit splitting	Branching ratio	Doniach-Sunjic	Lorentzian FWHM	Gaussian FWHM
Ag 3d	6.0 eV	1.5	0.067	0.27 eV	0.5 eV
Au 4f	3.66 eV	1.33	0.053	0.32 eV	0.5 eV

III. RESULTS

A. Elemental and chemical mapping

The interfaces under investigation contain 3D particles of micrometer and submicrometer dimensions, which are unevenly distributed and cover a very small fraction ($\leqslant$1%) of the surface. By tuning the analyzer to the Ag 3d, Au 4f, or Si 2p photoelectrons and scanning the sample, we obtained maps which reflect the distribution of the elements at the surface and near-surface region of the interface with spatial resolution of 0.15 μm. For all images presented in this paper the secondary electron background is subtracted.[23] Thus the contrast of the maps corresponds to the core-level peak intensity. Since the interaction of Ag and Au with Si results in a substantial chemical shift of the Ag 3d and Au 4f core levels ($\geqslant$0.8 eV), chemical mapping was performed as well, by tuning to the metallic or reacted components of the Ag 3d or Au 4f core-level peak. In addition to the information on the lateral distribution of the elements, imaging the interface is of fundamental importance for locating the different subphases (3D Ag islands and the $\sqrt{3}$ phase) and controlling the morphology variations during interface formation.

Figure 1 shows typical two-dimensional Ag micrographs of the initial $\sqrt{3}$-Ag interface with 3D islands. The brightness of the pixels reflects the intensity of the photoelectron signal, indicating that the imaged bright spots (3D Ag islands) con-

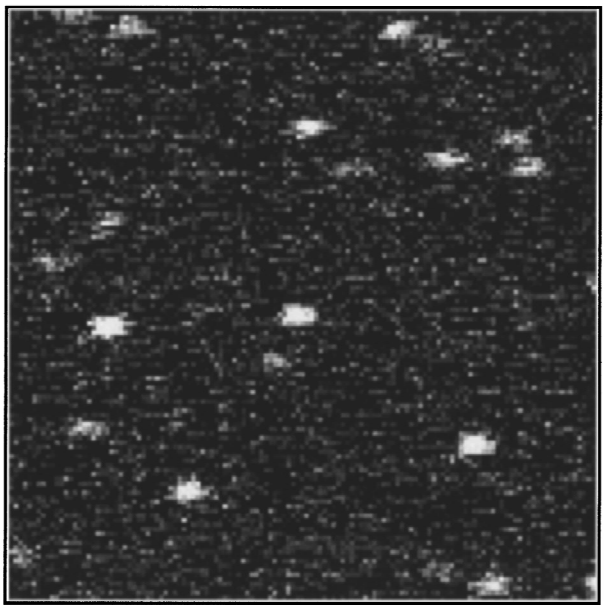

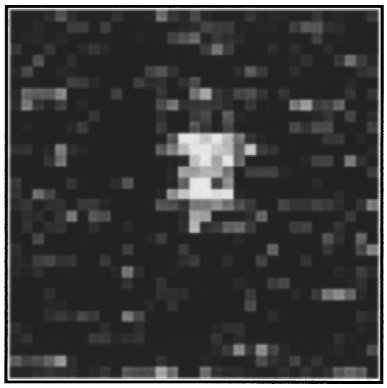

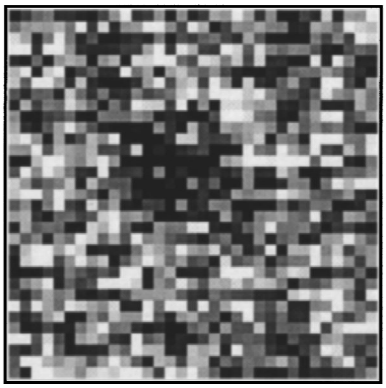

FIG. 1. (25.6×25.6)- (top) and (6.4×6.4)-μm^2 (bottom) Ag $3d_{5/2}$ maps of the initial $\sqrt{3}$-Ag/Si(111) interface. The two bottom images illustrate the reverse contrast obtained when the analyzer was tuned to the metallic (M) and the reacted (R) Ag $3d_{5/2}$ components.

tain more Ag than the flat areas. Maps tuned to the reacted Ag $3d_{5/2}$ component showed reverse contrast, indicating that the metallic Ag is present only in the 3D islands, whereas Ag in the $\sqrt{3}$ phase had reacted with Si, as can be seen in the two images in the bottom of Fig. 1. The Si $2p$ maps show similar depressions in the 3D areas as in the Ag-reacted maps because the thick Ag islands damp the Si substrate emission. The 3D island density and size varies with the amount of the deposited Ag. According to the SPEM images our initial $\sqrt{3}$-Ag/Si interfaces contained (1.9)–3.6×10^6 3D islands/cm^2 with an average diameter of $\sim$0.5–0.6 μm and a height of 500–600 Å.

The deposition of Au and following annealing did not result in dramatic changes in the contrast of the Ag $3d$ and Si $2p$ maps. Figure 2 illustrates chemical maps of the bimetal interface annealed to 860 K after deposition of 2 ML Au. The most important piece of information is the reverse contrast in the Au $4f$ chemical maps. It clearly shows that the 2D phase contains only reacted Au. These elemental and chemical maps were the starting base for an investigation of the local composition and processes in the 2D and 3D phases. The compositional difference pinpointed by imaging was quantified by analyzing the photoelectron spectra taken on the 2D and 3D areas selected from the maps.

B. Photoelectron spectroscopy from microareas on the sample

1. $\sqrt{3}$-Ag/Si interface with 3D Ag islands

Here the difference in the Ag chemical state in the 3D islands and $\sqrt{3}$-Ag phase, shown by Ag $3d$ core-level spectra on the bottom of Fig. 3, will be described in order to outline the features important for understanding the evolution of the interface after Au coadsorption. The Ag $3d$ spectra from the $\sqrt{3}$ phase, where all Ag atoms are bonded to Si, contain only a reacted (R) component, shifted by $+0.8$ eV with respect to the metallic Ag $3d$ binding energy. A small reacted component also exists in the Ag $3d$ spectra from the 3D islands where the metallic (M) component is dominant. The Si $2p$

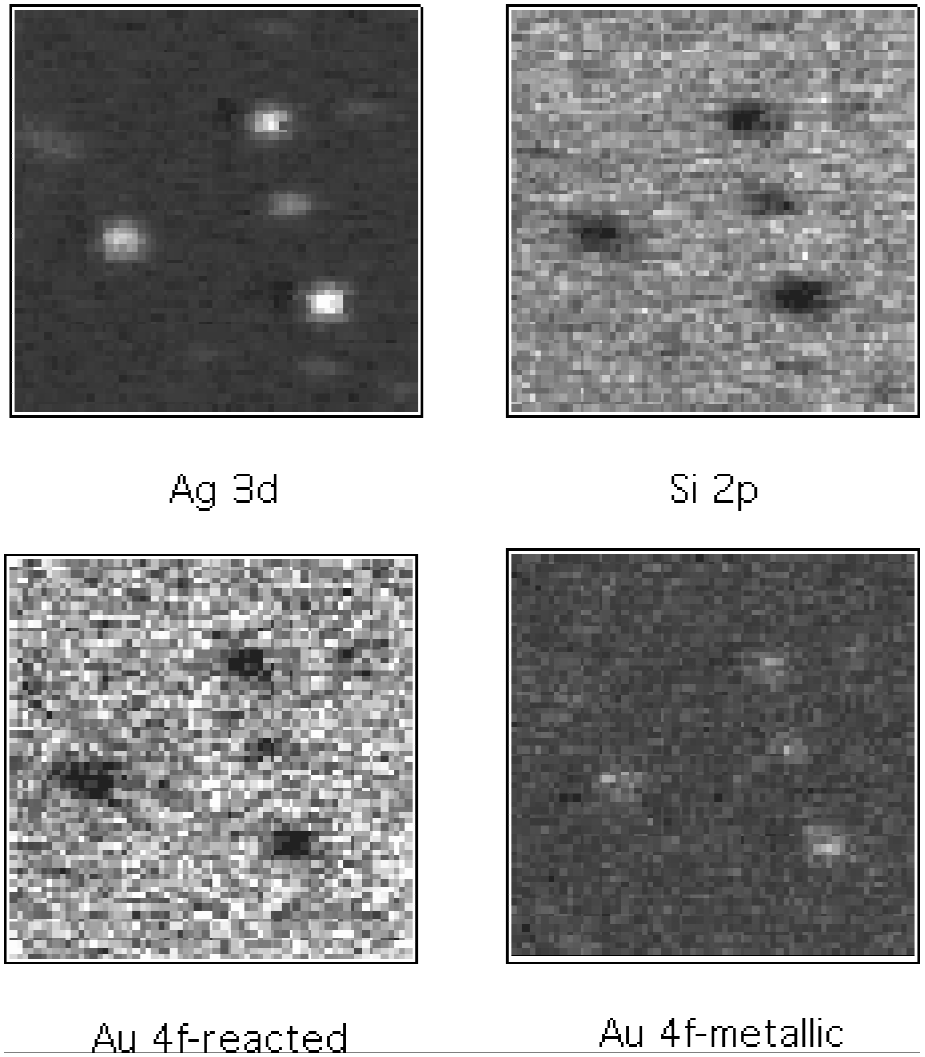

FIG. 2. (12.8×12.8)-μm^2 images of the Au-Ag/Si interface after annealing up to 860 K. The images are taken at Ag $3d$ and Si $2p$ (top), and the metallic or reacted component of the Au $4f$ core level (bottom).

PE spectra from the 3D islands also showed the presence of Si. This Si should be located on and near the surface of the 3D islands, because the thick Ag islands damp any photoemission from the substrate. By analyzing the intensities of the Ag and Si PE spectra using the procedures described in Sec. II and supposing that the R-Ag component is due to photoemission from the Si-coordinated Ag, led us to the conclusion that the Ag 3D islands should be covered by a thin $\sim1-2$ ML Ag_xSi_y film. Despite being highly immiscible in bulk, the observed surface-confined Ag_xSi_y phase is one more example of a system where the large atomic mismatch favors formation of a surface alloy.[24] A similar composition is found for the 3D Au islands in Au/Si(111) interface, but in this system the cover is much thicker: >4 ML of Au_xSi_y+ ~1 ML Si on top.[13,25] Both the thicker Au_xSi_y skin and the larger Au $4f$ chemical shift of the Au bonded with Si $(+1.1$ eV) are in agreement with the higher Au-Si affinity. The actual structure of the silicidelike phase covering the 3D metal islands is still unclear.

The valence-band spectra reveal that in contrast to the semiconducting $\sqrt{3}$-Ag/Si interface the 3D Ag phase is metallic (see Fig. 7). More details of the Ag/Si system along with some theoretical calculations will be given in Ref. 12. In the following sections we will follow the changes in the 2D and 3D Ag phases when adsorbing different quantities of Au, and when annealing the bimetal interface to different temperatures.

2. Core-level spectromicroscopy from the bimetal interface after Au deposition at 300 K

The effect of Au coverage deposited at 300 K on the Au $3d$ and Au $4f$ PE spectra can be seen in Fig. 3. In order to outline the line-shape changes, which reflect the actual chemical state of the metals, different scales are used for plotting the Ad $3d$ and Au $4f$ spectra. There is a distinguishable difference in the evolution of the Ag $3d$ and Au $4f$ spectra from the $\sqrt{3}$-Ag and 3D Ag islands with increasing Au coverage.

The evolution of the spectra from the initial $\sqrt{3}$-Ag areas can be summarized as follows. After deposition of 0.7 ML Au a M-Ag component appears in the Ag $3d$ spectra and the shift of the R-Ag decreases from 0.8 to 0.55 eV. The Au $4f$ spectra contain only a R-Au component. LEED of this bimetal interface shows an appearance of faint additional spots, belonging to a $(2\sqrt{3}\times2\sqrt{3})$ pattern, which become sharp after annealing to 470 K. After annealing to 470 K the Ag $3d$ and Au $4f$ spectra remain almost intact, indicating that the 470-K annealing only improves the long-range order of the $2\sqrt{3}$-(Au+Ag) layer. The R-Ag component completely disappears after deposition of 2 ML Au, whereas the

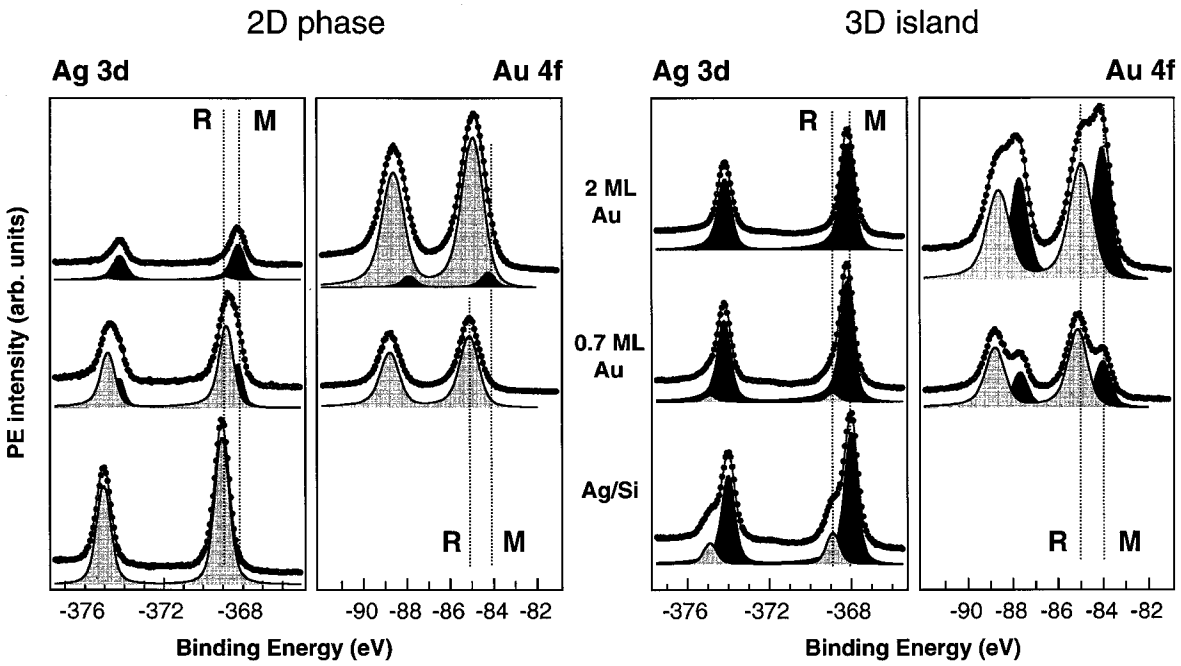

FIG. 3. Ag $3d$ and Au $4f$ core-level spectra taken before (bottom spectra) and after adsorption of 0.7 (middle spectra) and 2 ML (top spectra) of Au at 300 K on the $\sqrt{3}$-Ag/Si(111) interface. Left and right panels show the spectra taken from the 2D and 3D phases, respectively. The metallic (M) and reacted (R) components are shaded dark and light grey, respectively.

R-Au component remains dominant in the Au $4f$ spectra. No LEED pattern was observed after deposition of 2 ML Au, which indicates a disordered surface. This lack of a long-range order is consistent with the rather broad R-Au component, indicative of a variety of Au-Si coordinations.

The important piece of information carried out by the intensity variations of the Ag $3d$, Au $4f$, and Si $2p$ spectra from the 2D phase can be summarized as follows. The Si $2p$ peak intensity attenuates almost within the expected quantity predicted by the electron free mean path for 0.7 and 2 ML Au on top. The Ag and Au intensity variations deviate from this simple model. The Ag/Au intensity ratio after deposition of 0.7 ML Au corresponds to the actual amount of the two metals: 1/0.7. This indicates that the Au and Ag atoms should be almost in the same plane. When increasing the Au coverage to 2 ML the Ag $3d$ peak loses $\sim$70% of its intensity, whereas the Au $4f$ intensity grows almost proportionally to the amount of deposited Au atoms. It is notable that in this case the PE spectra in Fig. 3 show only metallic Ag, whereas most of Au remains in a reacted state.

The spectra from the 3D islands [Fig. 3(b)] show that the R-Ag component is already drastically reduced by 0.7 ML Au. In contrast, the Au $4f$ spectra contain both R-Au and M-Au components, the latter growing faster with increasing Au coverage.

Our energy resolution is not sufficient to fit the Si peak precisely enough in order to obtain quantitative evaluations. However, the Si $2p$ spectra in Fig. 4(a) show that the deposition of Au results in changes which can be described as conversion to a shape similar to that of a Au/Si interface. Note that the band bending (0.59 and 0.4 eV, respectively) and the energy shifts and weight of the surface and bulk components are different for the $\sqrt{3}$-Au/Si and Ag/Si interfaces.[26,27] This accounts for the different line shape of the Si $2p$ spectra from the $\sqrt{3}$-Ag/Si and Au/Si interfaces. The broad Si $2p$ spectrum taken from the disordered interface after deposition of 2 ML Au implies a variety of chemically different Si species.

3. Core-level spectromicroscopy from the bimetal interface after annealing to different temperatures

Annealing the bimetal interface after deposition of 2 ML Au led to remarkable differences in the core-level evolution of the two subphases. The dominating 2D phase also undergoes structural changes, as shown by the LEED patterns. Figure 5 shows the Ag $3d$ and Au $4f$ core-level spectra taken after annealing to different temperatures. The peak intensity changes, and the LEED patterns, observed after each annealing stage, are shown as bar chart diagrams in Fig. 6. In the case of Ag and Au the intensity variations of the M and R components are presented separately. For an easier comparison, the Ag $3d$ and Si $2p$ data for the initial $\sqrt{3}$-Ag phase are also shown.

The spectra in Fig. 5(a) and the core-level intensity changes, summarized in Fig. 6(a), show the following temperature effects on the 2D phase. The Ag $3d$ core levels, which contain only a M-Ag component after deposition of 2 ML Au, undergo a positive binding-energy shift of 0.7–0.8 eV on annealing. The spectra after annealing to 770 K show that the M-Ag was completely displaced by R-Ag, accompanied by an intensity gain. After annealing to 860 K, the R-Ag component intensity becomes comparable to that of the initial $\sqrt{3}$-Ag/Si(111) interface. Above 860 K, Ag starts to desorb from the surface, so that the Ag $3d$ spectra show no Ag after annealing to 1030 K. The changes in the Au $4f$ line shape upon annealing are confined only in sharpening of the peaks with small upward energy shift of the R-Au compo-

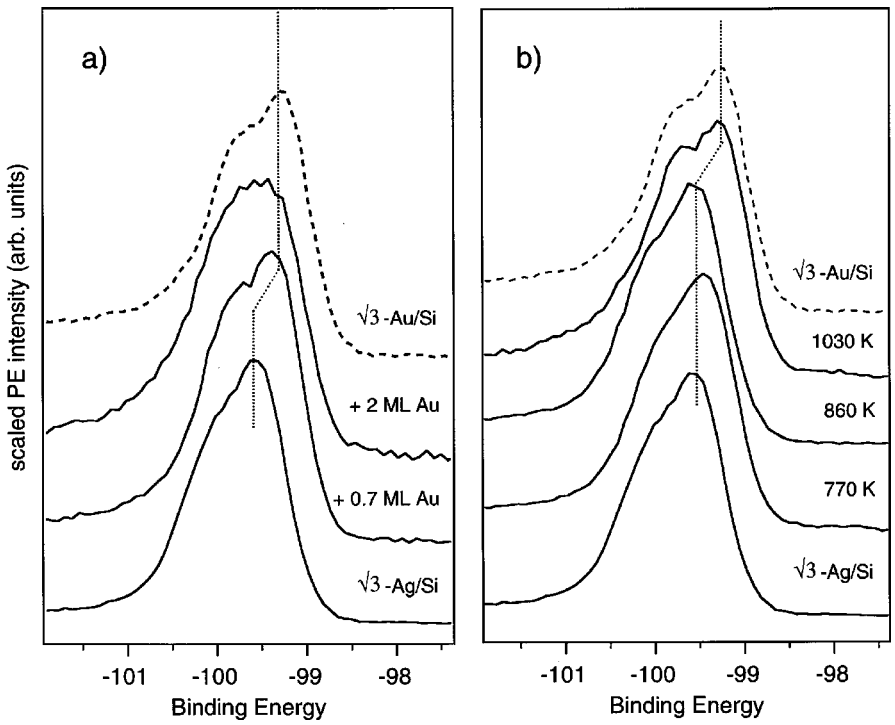

FIG. 4. (a) The evolution of the Si $2p$ spectra from the 2D $\sqrt{3}$-Ag phase with increasing Au coverage at 300 K. (b) The evolution of the Si $2p$ spectra from the 2D phase with 2 ML Au with increasing temperature. All spectra are scaled to 100% in order to outline the peak shape changes. The Si $2p$ spectra from a $\sqrt{3}$-Au/Si(111) interface is shown by a dashed line for the sake of comparison. In both panels the bottom spectra correspond to the initial 2D $\sqrt{3}$-Ag phase.

nent. More drastic are the intensity changes: the Au $4f$ intensity decreases by ~ 6 times with increasing annealing temperature to 860 K. After desorption of Ag the Au $4f$ peak gains back intensity, reaching the value of the $\sqrt{3}$-Au phase with ~ 1 ML Au. The Si $2p$ peak already retains its intensity of the initial $\sqrt{3}$-Ag/Si(111) already after annealing up to 770 K, and does not change with further annealing. The Si $2p$ peak shape changes upon annealing, as displayed in Fig. 4(b): it becomes $\sqrt{3}$-Ag/Si like at 770 and 860 K. Only after Ag desorption at 1030 K does the Si $2p$ peak become nearly identical to the one of the $\sqrt{3}$-Au/Si interface.

Inspecting the evolution of the core-level spectra from the 3D phase in Fig. 5(b) shows that the major changes are undergone by the Au $4f$ spectra. The R-Au and M-Au components become sharper and better resolved with small gain in the relative weight of the R-Au when annealed to 860 K.

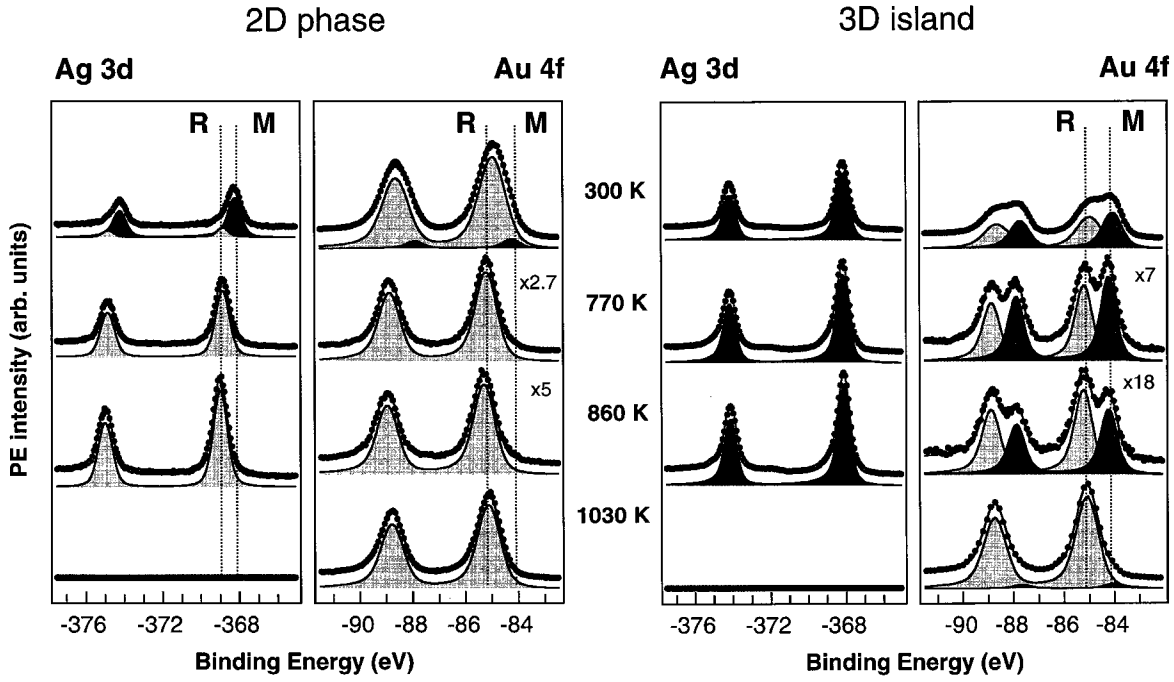

FIG. 5. The evolution of the Ag $3d$ and Au $4f$ spectra with annealing of the 2 ML Au-Ag/Si interface. Left and right panels show the spectra taken from the 2D and 3D phases, respectively. The metallic (M) and reacted (R) components are shaded dark and light grey, respectively. The intensities are comparable only inside each chart.

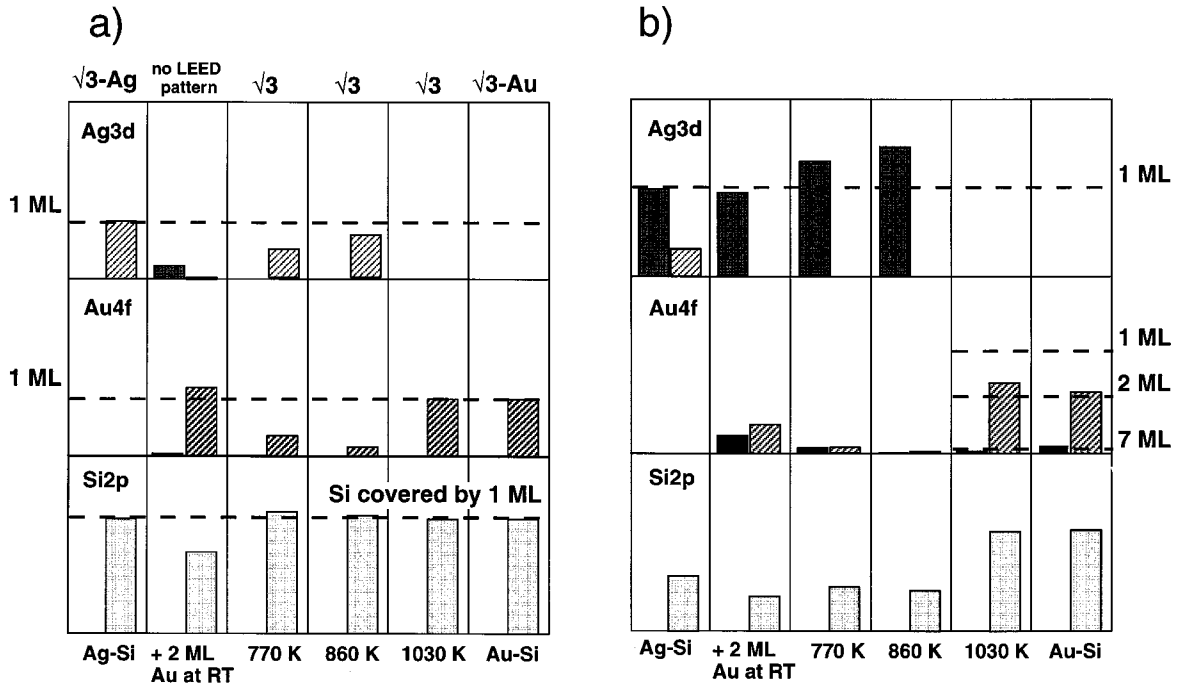

FIG. 6. The normalized Ag, Au, and Si peak intensities measured at the (a) 2D and (b) 3D phases. The metallic (black) and the reacted (hatched) components of Au $4f$ and Ag $3d$ are displayed separately in the charts. For comparison, the Ag $3d$ and Au $4f$ intensities of the $\sqrt{3}$-Ag/Si(111) and the $\sqrt{3}$-Au/Si(111) structures are added. In the bottom of (a) and (b), the preparation of each surface is outlined. The corresponding LEED pattern obtained for each surface is displayed in the top of each chart. In (a) the dashed line indicates the expected intensity of the corresponding $\sqrt{3}$-metal structure. In (b) the dashed lines indicate the expected intensities if 1–7 monolayers of another species are present on top of a metallic 3D island.

After Ag desorption the R-Au component remains dominant in the Au $4f$ spectra. These line-shape changes are accompanied by rather dramatic intensity changes, as illustrated in Fig. 6(b). The Au $4f$ intensity drops $\sim$9 times on annealing to 860 K. After Ag desorption only the R-Au component grows, attaining an intensity beyond the initial value. The Ag $3d$ core-level changes consist of the emergence of a very weak R-Ag component and a substantial, up to $\sim$50%, intensity increase upon annealing to 860 K. Only traces of Ag close to the resolution limit of our instrument remain in the Ag $3d$ region after annealing to 1030 K. The Si intensity remains almost constant up to 860 K. A pronounced increase of the Si $2p$ intensity was seen after annealing to 1030 K.

4. Valence-band spectra

The difference in the local electronic structure of the initial $\sqrt{3}$-Ag and 3D phases and the changes induced by Au deposition and annealing are clearly manifested by the valence-band (VB) spectra in Fig. 7. We would like to note that our experimental setup does not permit high energy and angular resolution for a detailed description of the electronic structure, but two features can be clearly distinguished in the valence-band spectra: the Ag $4d$-band-width and the density of states near the Fermi edge.

The VB changes of the 2D phase are significant. As can be seen in Fig. 7 the initial $\sqrt{3}$-Ag phase is characterized by a narrow Ag $4d$ band, due to the weak Ag-Ag interactions between the distanced Ag adatoms, and a gap at the Fermi edge consistent with the reported semiconductivity of the $\sqrt{3}$-Ag surface.[9,10] The deposition of 2 ML Au at 300 K converts the interface into a metalliclike one with overlapping Ag $4d$ and Au $5d$ bands. Annealing the bimetal interface to 770 and 860 K causes a drastic reduction of the states at the Fermi edge of the 2D phase, resulting in a VB similar to the initial $\sqrt{3}$-Ag one. After desorption of Ag at 1030 K, the VB is identical to the one of the $\sqrt{3}$-Au/Si(111).

The VB of the 3D Ag phase is similar to the Ag bulk VB spectrum. The overlap between the Ag $4d$ and Au $5d$ bands after Au deposition and annealing accounts for the changes in the d-band width and line shape. The latter vary with the relative weight of the Au-related component, i.e., with the amount of Au in the surface and near-surface region. Desorption of Ag results in a VB spectrum characteristic for the 3D Au phase. Note that the d-band line shape and width of the VB spectra from the 3D islands differs from that of the pure Au due to the presence of p-d hybridized states from the Au_xSi_y skin.

IV. DISCUSSION

A. Effect of the Au coverage on the local Au-Ag/Si(111) interface composition and structure

The changes in the Ag $3d$, Si $2p$, and Au $4f$ line shapes and intensities with increasing Au coverage at 300 K clearly manifest the difference in the behavior of the $\sqrt{3}$-Ag and 3D Ag adislands. The spectral analyses show that the process controlling the evolution of both subphases at 300 K is the displacement of Ag bonded to Si by Au. This is in accor-

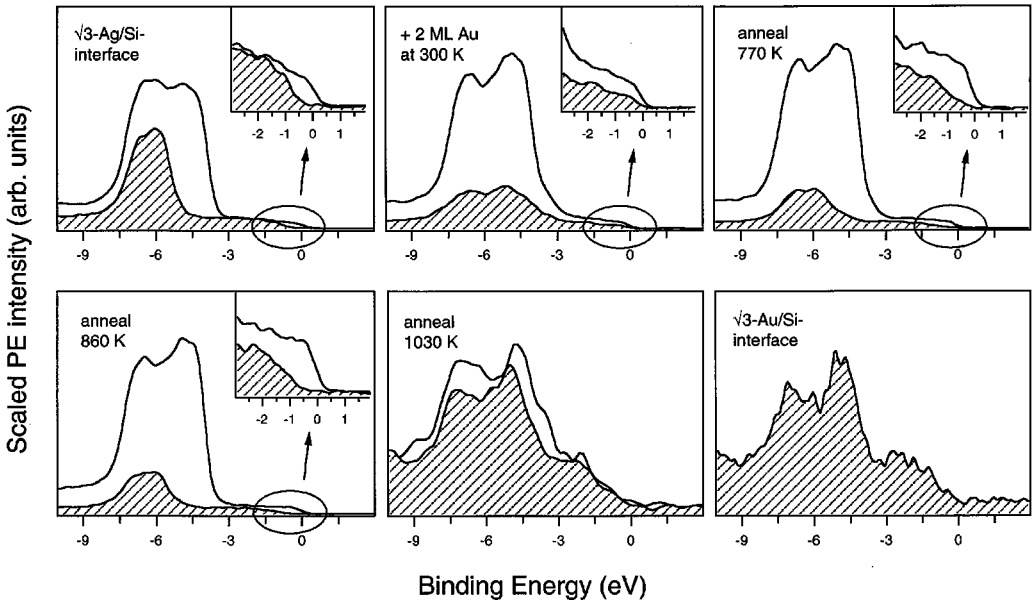

FIG. 7. Valence-band (VB) spectra taken from the 2D (hatched) and 3D phases. All spectra are scaled to 100%. Note the different electronic structure of the two phases near the Fermi-edge region, shown in the insets in detail. The VB spectra from the clean $\sqrt{3}$-Ag/Si or $\sqrt{3}$-Au/Si interface are shown for comparison.

dance with the higher affinity of Au to Si. This results in disappearance of the R-Ag component from the Ag $3d$ spectra, the continuous presence of a R-Au component in the Au $4f$ spectra, and the conversion of the Si $2p$ line shape into a Au/Si-like one.

The exchange of Ag by Au in the silicide phase occurs on the 3D islands with the first doses of Au. Ag is readily released from the Ag_xSi_y phase covering the 3D Ag islands, and a Au silicide cover is formed instead. The excess of Au remains metallic, and likely alloys with Ag. As observed in the reverse deposition mode, AgAu alloying was the only process occurring in the 3D Au adislands after Ag deposition at 300 K.[25] Since the chemical shift of the Au $4f$ levels upon alloying is very small ($\leqslant +0.1$ eV) it cannot be easily distinguished.[28]

Analysis of the PE spectra and the structural rearrangement, shown by LEED, indicate that in contrast to the 3D phase the $\sqrt{3}$-Ag/Si(111) interface can accommodate an additional ~ 0.7 ML of Au, forming an ordered $(\sqrt{3}\times 2\sqrt{3})R30°$ mixed structure. Previous structural studies showed that adding $\frac{1}{7}$ ML Au to the $\sqrt{3}$-Ag/Si(111) surface results in a $(\sqrt{21}\times\sqrt{21})R10.89°$ structure with Au atoms probably located on top of some Si trimers.[29,30] Increasing the Au coverage to $\frac{1}{3}$ ML, all Si trimers are occupied, resulting in a new $(\sqrt{3}\times\sqrt{3})R30°$-(Au+Ag) LEED pattern.[30] We suggest here that incorporating another $\frac{1}{3}$ ML Au in the $\sqrt{3}$-Au+Ag adlayer the structure shown in Fig. 8 can be formed. As illustrated in Fig. 8, the most symmetrical way to accommodate another $\frac{1}{3}$ ML Au is to place one Au atom inside the $(\sqrt{3}\times\sqrt{3})$-(Au+Ag) unit cell. Altering its position leads to a $(\sqrt{3}\times 2\sqrt{3})R30°$ structure. Rotational domains result in the observed $(2\sqrt{3}\times 2\sqrt{3})R30°$ LEED pattern.

Inside the $(\sqrt{3}\times 2\sqrt{3})$ unit cell of Fig. 8, the Ag atoms are differently coordinated: one Ag adatoms is coordinated by three Au atoms, two Ag atoms are coordinated by two Au, atoms and three Ag atoms are attached to one Au atom. This different environment of the Ag atoms is consistent with the line shape of the Ag $3d$ spectra. The reduced chemical shift of the R-Ag component with respect to the $\sqrt{3}$-Ag phase can be interpreted as a weakening of the Ag-Si coupling because of arising Ag-Au interactions in the rather dense adlayer. Considering the Au and Ag atomic sizes, the Ag atoms coordinated by three Au atoms should be displaced vertically and decoupled from the Si surface. The emitted Ag $3d$ photoelectrons from these atoms give rise to the small M-Ag in the Ag $3d$ spectra. Also, the Si trimers do not necessarily have to remain, as pointed out in Ref. 28 regarding the less dense $\sqrt{21}$- and $\sqrt{3}$-(Ag+Au) structures.

It should be noted that, for the $(\sqrt{21}\times\sqrt{21})R10.89°$ structure Nogami, Wan, and Lin proposed that the Au atoms are located above the center of three neighboring Ag atoms rather than on the Si trimers.[31] We do not favor this model because in this case, the Au atoms are bonded only to Ag, which contradicts the observed pronounced shift of the Au $4f$ core-level peak.

The driving force for the replacement of Ag from the $2\sqrt{3}$-(Ag+Au) adlayer by Au at Au coverages higher than ~ 0.6 ML should be the energy gain given by the difference ΔE between the bond strengths, $E_{\text{Si-Ag}}$ and $E_{\text{Si-Au}}$. The present data indicate that the $E_{\text{Si-Ag}}$ is Au coverage dependent, so that ΔE becomes negative above a certain Au coverage. This is consistent with the reduced degree of Ag-Si coupling with an increasing number of Au adatoms, shown for the $2\sqrt{3}$-(Ag+Au) phase. The above assumption that Ag coordinated with three Au adatoms is locally decoupled from Si means that by incorporation of only two more Au atoms in the $2\sqrt{3}$ unit cell, i.e., deposition of additional $\frac{1}{3}$ ML Au, all Ag adatoms should be decoupled from a Si surface. The Ag displacement, shown by the extinction of the R-Ag component in the Ag $3d$ spectra, is accompanied by disruption of the dense $2\sqrt{3}$-(Ag+Au) ordered layer. The Au $4f$ as well as Si $2p$ line shapes and intensities are consistent with the formation of a dense disordered 2D Au layer on top of Si,

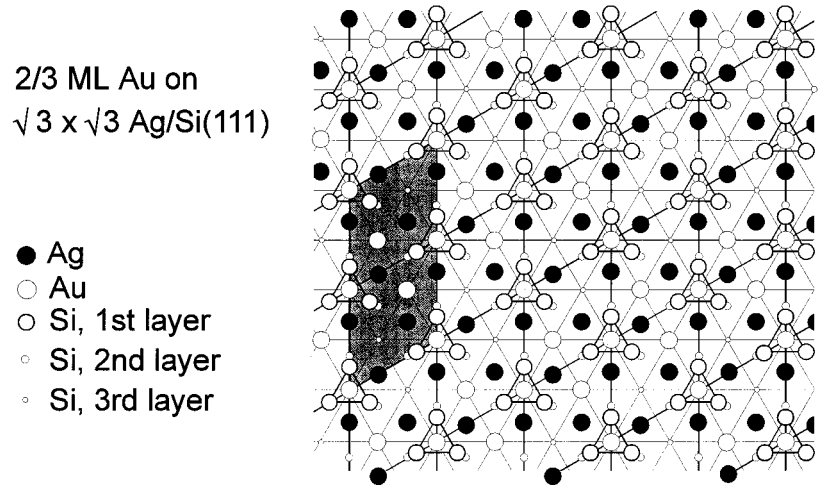

FIG. 8. Proposed structure of the Ag/Si(111)-($\sqrt{3}\times\sqrt{3}$)$R30°$ interface after adsorption of $\frac{2}{3}$-ML Au. Rotational domains of the ($\sqrt{3}\times 2\sqrt{3}$)$R30°$ unit cell cause the observed ($2\sqrt{3}\times 2\sqrt{3}$)$R30°$ LEED pattern. Note that there are Ag atoms completely and partly surrounded by Au atoms.

which contains ~1.7 ML Au, the same coverage as that of the $2\sqrt{3}$-(Au+Ag) adlayer. This suggests that ~1.7 ML is the maximum density of a Au or Au+Ag adatoms that can reside on the Si(111) surface, a value comparable with the atomic density, 1.8 ML, of the Au(111) plane. The suggestion that the displacement of Ag starts above ~0.6 ML Au was confirmed by our most recent experiments: depositing a patch of 2 ML Au onto a $\sqrt{3}$-Ag interface, and annealing, we produced a Au gradient Au from 0 to 2 ML, which allowed us to follow the variation of the local composition moving away from the patch.[32]

A surprising result is the pronounced Ag $3d$ intensity loss which accompanies the displacement of Ag from the Si surface. This can be described consistently, assuming only clustering of the expelled Ag atoms on top of the Au/Si interface in accordance with the SEM measurements which show the appearance of nm-sized islands.[14,15] This result reveals that Ag cannot wet the amorphous Au adlayer, where all Au is in contact with the Si surface, and tends to form 3D nucleates. In the framework of free energy changes, the formation of 3D islands is favored if $F_{\mathrm{Ag}}+F_i-F_{\mathrm{Au}}>0$, where F_i is the interface free energy. Since for pure Au and Ag $F_{\mathrm{Ag}}<F_{\mathrm{Au}}$,[33] the Ag agglomeration suggests that the free energy of the dense Au 2D layer on Si, F_{Au}, is smaller than that of pure Au, or/and $F_i>0$.

The quite different reactivity of the 2D and 3D phases with respect to Ag displacement at Au coverages less than ~0.7 ML can be attributed to the structure and Ag-Si bond strength in the $\sqrt{3}$-Ag and in the 3D phases. In the 3D phase the Ag_xSi_y is probably in amorphous form (solid solution) with undefined Ag coordination. In the $\sqrt{3}$-Ag/Si structure an optimal Ag-Si coupling conditions are attained, where the large Ag-Ag separation (3.4 Å) minimizes the Ag-Ag interactions. The $\sqrt{3}$-Ag structure also permits incorporation of additional metal atoms which bond to Si, whereas in the Ag_xSi_y solid solution Ag and Si are more densely packed and the formation of the Au-Si bond supposes substitution of Ag.

The changes in the VB spectra after Au deposition are in excellent agreement with the changes in the core-level spectra, and support the suggested evolution of the interface. The conversion of the VB of the 2D $\sqrt{3}$-Ag interface to a Au/Si-like one is consistent with the displacement of the Ag from the Si surface by a dense disordered Au adlayer. This converts the interface into metallic and the d band is very similar to the Au $5d$ band observed for ~2-ML room temperature grown Au film.[34] The dominance of the Au-related valence-band features also supports the model for formation of Ag clusters which covers small fraction of the surface, so that the contribution from Ag $4d$ band to the PE spectra is small.

B. Temperature-induced rearrangements in the 2D and 3D phases

The information carried out by the changes in the line-shape and intensity of the Ag, Au, and Si core-level spectra after annealing and the structures shown by LEED reveal rather peculiar properties of the 2D phase. In contrast to the expected evolution considering the Au-Si (2.5 eV) and Ag-Si (0.8 eV) bond strengths in the corresponding $\sqrt{3}$ phases,[16] the annealing results in the formation of an Ag-dominated $\sqrt{3}$ phase containing ~0.8 ML Ag and ~0.2 ML Au (see Fig. 6).

Detailed $I-V$ LEED studies are necessary to distinguish between the two possible arrangement of the Ag and Au adatoms in the $\sqrt{3}$ layer: Au randomly distributed in the $\sqrt{3}$-Ag phase or separate $\sqrt{3}$-Ag/Si(111) and $\sqrt{3}$-Au/Si domains. However, the almost identical VB spectra and Si $2p$ peak shapes of the initial $\sqrt{3}$-Ag and the ones formed after annealing the $\sqrt{3}$-(Au+Ag) interface up to 860 K show that the electronic structure of the latter is almost identical to the $\sqrt{3}$-Ag/Si one. This means that the minority Au adatoms are randomly distributed, replacing some Ag in the $\sqrt{3}$-Ag phase.

This result indicates that, although thermodynamically favored, the conversion of the amorphous dense Au adlayer, formed after displacement of Ag by Au at 300 K, into a reconstructed $\sqrt{3}$-Au phase is kinetically hindered. Indeed, the temperatures required for the formation of a $\sqrt{3}$-Ag($\geq$470 K) or $\sqrt{3}$-Au(>700 K) phase indicate a higher activation barrier in the latter case. Another competing pro-

cess, which takes place when annealing Au films on Si(111), is Au agglomeration in 3D islands.[35] The present system already contains 3D islands which can act as centers to promote Au agglomeration. Au agglomeration in the existing Ag islands is also thermodynamically favorable because of the energy gain from Au-Ag alloying. Apparently the Au agglomeration dominates in the temperature range 700–860 K, consuming a large fraction of the deposited Au. Since the annealing temperatures are close to the Ag desorption temperatures, the Ag atoms are much more mobile than Au, and most of the liberated sites on the Si surface are naturally occupied by Ag.

The processes controlling the changes in the surface and subsurface compositions of the 3D islands are quite different from those in the 2D phase. The fast attenuation of the Au $4f$ signal indicates that, upon annealing, Au sinks deeper into the 3D islands, where alloying with Ag is thermodynamically and kinetically favorable even at room temperature.[17,36] This decrease of the Au amount on top the Ag-rich islands naturally results in an increase of the Ag $3d$ photoelectron yield. The annealing also induces changes in the AgAuSi skin covering the 3D islands, as shown by the Si $2p$ and Au $4f$ spectra: the Si $2p$ intensity stays nearly constant, whereas the R-Au component becomes sharper but loses intensity. According to the evolution of the Au, Ag, and Si core-level spectra, the annealing causes a reduction in the Au content of the metal-silicide cover. Assuming that the position of the R-Au with respect to the M-Au correlates with the number of Si per Au, the sharper R-Au component peaked at higher binding energy after annealing is consistent with the reduced Au/Si ratio in the skin. A result that deserves some comment is the invariance of the Si quantity in the topmost layers of the $3d$ islands up to 860 K (see Fig. 6). This temperature markedly exceeds the Au-Si eutectic point of 670 K. In the monocomponent Au/Si system the interface between the Au 3D islands and Si becomes liquidlike at $T \geqslant 670$ K.[35] Si enrichment of the topmost layer and enhancement of the Au_xSi_y skin thickness was evidenced with further increasing the temperature.[13,17] In the present system, enhancement of the Si outdiffusion occurs only after desorption of Ag, i.e., after annealing to 1030 K. This is consistent with the pronounced thickness of the Ag 3D islands, which constrains the post-deposited Au atoms from easily reaching the Si substrate. Only after removal of Ag can burrowed (and alloyed with Ag) Au atoms come in contact with Si, resulting in a distinctive change of the 3D phase near-surface composition. Considering the damping of the M-Au peak, we estimated that after Ag desorption the 3D islands are covered by a $\sim$7-ML-thick Au-Si skin. This is in fair agreement with previous studies on a monocomponent Au/Si interface where a AuSi skin of 4–6 ML was formed in a single 870-K annealing step of a 6-ML Au/Si room temperature interface.[17]

V. CONCLUSIONS

With the help of a laterally resolving photoemission microscope we investigated the structural and compositional changes of the Au-Ag/Si interfaces, and related them to the different processes occurring in the 2D and 3D phases of this interface. It was shown that at 300 K the Ag/Si(111)-$(\sqrt{3}\times\sqrt{3})R30°$ surface can accommodate an additional 0.7 ML Au, resulting in an ordered $(\sqrt{3}\times 2\sqrt{3})R30°$ structure. When exceeding this Au coverage the Ag atoms are repelled from the Si interface, and replaced by the Au atoms. Although the Ag-Si interface of the 2D phase is nearly removed after deposition of 2 ML Au at 300 K, a two-dimensional ordered phase similar to the starting one can be nearly restored after annealing up to 860 K. We suggest that the key processes in the interface evolution are the transport of Au atoms from the 2D phase toward the 3D islands, and the strength of the Si-Au interactions. We showed that the electronic properties of the different bimetal-Si interfaces are in agreement with their proposed structural changes.

ACKNOWLEDGMENTS

We would like to thank the entire staff of the ELETTRA synchrotron radiation facility, especially Diego Lonza and Gilio Sandrin, for their excellent technical support. The work was supported by an EC grant under Contract No. ERBCHGECT920013 and by Sincrotrone Trieste SCpA.

*Present address: Institute of Surface Engineering and Optoelectronics, Teslova 30, Ljubliana, Slovenia.

[1] G. Le Lay and J. P. Faurie, Surf. Sci. **69**, 295 (1977).
[2] D. Dornisch, W. Moritz, H. Schulz, R. Feidenhansl, M. Nielsen, F. Grey, and R. L. Johnson, Phys. Rev. B **44**, 11 221 (1991).
[3] M. Hanbücken, M. Futamoto, and J. A. Venables, Surf. Sci. **147**, 433 (1984).
[4] Y. G. Ding, C. T. Chan, and K. M. Ho, Surf. Sci. Lett. **275**, L691 (1992).
[5] K. J. Wan, X. F. Lin, and J. Nogami, Phys. Rev. B **47**, 13 700 (1993).
[6] Y. G. Ding, C. T. Chan, and K. M. Ho, Phys. Rev. B **67**, 1454 (1991).
[7] G. Raynerd, M. Hardiman, and J. A. Venables, Phys. Rev. B **44**, 13 803 (1991).
[8] A. Endo and S. Ino, Surf. Sci. **293**, 165 (1993).
[9] S. Kono, K. Higashiyama, T. Kinoshita, T. Miyahara, H. Kato, H. Ohsawa, Y. Enta, F. Maeda, and Y. Yaegashi, Phys. Rev. Lett. **58**, 1555 (1987).
[10] L. S. O. Johansson, E. Landemark, C. J. Karlsson, and R. I. G. Uhrberg, Phys. Rev. Lett. **63**, 2092 (1989).
[11] L. Casalis *et al.*, Rev. Sci. Instrum. **66**, 4870 (1995).
[12] M. Sancrotti *et al.* (unpublished).
[13] S. Vandre', E. Narducci, A. Goldoni, C. Lenardi, L. Calliari, L. Casalis, L. Gregoratti, J. Kovac, M. Kiskinova, and M. Sancrotti, Surf. Sci. **377-379**, 266 (1997).
[14] A. Endo, Surf. Sci. **297**, 71 (1993).
[15] T. Yamanaka, A. Endo, and S. Ino, Surf. Sci. **294**, 53 (1993); S. Ino and T. Yamanaka, *ibid.* **298**, 432 (1993).
[16] J. Yuhara, M. Inoue, and K. Morita, J. Vac. Sci. Technol. A **11**, 2714 (1993).
[17] A. Kolmakov, J. Kovac, S. Günther, L. Casalis, L. Gregoratti, M. Marsi, and M. Kiskinova, Phys. Rev. B **55**, 4101 (1997).
[18] J. A. Venables, J. Derrien, and A. P. Janssen, Surf. Sci. **95**, 411 (1980).
[19] M. P. Seah and W. A. Dench, Surf. Interface Anal. **I**, 2 (1970).
[20] S. Tanuma, C. J. Powell, and D. R. Penn, Surf. Interface Anal. **11**, 577 (1988).

[21] T. Takahashi and S. Nakatani, Surf. Sci. **282**, 17 (1993).
[22] Y. Kuwahara, S. Nakatani, M. Takahasi, M. Aono, and T. Takahashi, Surf. Sci. **310**, 226 (1994).
[23] M. Marsi, L. Casalis, L. Gregoratti, S. Günther, A. Kolmakov, J. Kovac, D. Lonza, and M. Kiskinova, J. Electron Spectrosc. Relat. Phenom. (to be published).
[24] J. Tersoff, Phys. Rev. Lett. **74**, 434 (1995).
[25] A. Kolmakov, S. Günther, J. Kovac, M. Marsi, L. Casalis, K. Kaznacheev, and M. Kiskinova, Surf. Sci. (to be published).
[26] T. Okuda, H. Daimon, H. Shigeoka, Sh. Suga, T. Kinoshita, and A. Kakizaki, J. Electron Spectrosc. Relat. Phenom. **80**, 229 (1996).
[27] G. S. Herman, J. C. Woicik, A. B. Andrews, and J. L. Erskine, Surf. Sci. Lett. **290**, L643 (1993).
[28] C. C. Tyson, A. Bzowsky, P. Kristof, M. Kuhn, R. Sammynaiken, and T. K. Sham, Phys. Rev. B **45**, 8924 (1992).
[29] Y. L. Gavriljuk, V. G. Lifshits, and N. Enebish, Surf. Sci. **297**, 345 (1993).
[30] A. Ichimiya, H. Nomura, Y. Ito, and H. Iwashige, J. Cryst. Growth **150**, 1169 (1995).
[31] J. Nogami, K. J. Wan, and X. F. Lin, Surf. Sci. **306**, 81 (1994).
[32] M. Kiskinova *et al.* (unpublished).
[33] F. R. de Boer and D. G. Pettifor, *Cohesion and Structure* (North-Holland, Amsterdam, 1988), Vol. 1.
[34] S. L. Molodtsov, C. Laubschat, G. Kaindl, A. M. Shikin, and V. K. Adamchuk, Phys. Rev. B **44**, 8850 (1991).
[35] W. Swiech, E. Bauer, and M. Mundschau, Surf. Sci. **253**, 283 (1991).
[36] R. G. Kirsch, J. M. Poate, and M. Eibsehuts, Appl. Phys. Lett. **29**, 772 (1976).